De Novo Design of Strand-Swapped β-Hairpin Hydrogels

Radhika P. Nagarkar,[‡] Rohan A. Hule,[†] Darrin J. Pochan,[*,†] and
Joel P. Schneider[*,‡]

*Departments of Chemistry and Biochemistry and Materials Science and Engineering and the
Delaware Biotechnology Institute, University of Delaware, Newark, Delaware 19716*

Received November 29, 2007; E-mail: schneijp@udel.edu; pochan@udel.edu

Abstract: De Novo designed peptides, capable of undergoing a thermally triggered β-strand-swapped self-assembly event leading to hydrogel formation were prepared. Strand-swapping peptide 1 (SSP1) incorporates an exchangeable β-strand domain composed of eight residues appended to a nonexchangeable β-hairpin domain. CD shows that, at pH 9 and temperatures less than 35 °C, this peptide adopts a random coil conformation, rendering it soluble in aqueous solution. On heating to 37 °C or greater, SSP1 adopts a β-hairpin that displays an exchangeable β-strand region. The exchangeable strand domain participates in swapping with the exchangeable domain of another peptide, affording a strand-swapped dimer. These dimers further assemble into fibrils that define the hydrogel. A second peptide (SSP2) containing an exchangeable strand composed of only four residues was also studied. Microscopy and scattering data show that the length of the exchangeable domain directly influences the fibril nanostructure and can be used as a design element to construct either twisted (SSP1) or nontwisted (SSP2) fibril morphologies. CD, FTIR, and WAXS confirm that both peptides adopt β-sheet secondary structure when assembled into fibrils. Fibril dimensions, as measured by TEM, AFM, and SANS indicate a fibril diameter of 6.4 nm, a height of 6.0 nm, and a pitch of 50.4 nm for the twisted SSP1 fibrils. The nontwisted SSP2 fibrils are 6.2 nm in diameter and 2.5 nm in height. Oscillatory rheology, used to measure bulk hydrogel rigidity, showed that the gel composed of the nontwisted fibrils is more mechanically rigid (517 Pa at 6 rad/s) than the gel composed of twisted fibrils (367 Pa at 6 rad/s). This work demonstrates that β-strand-swapping can be used to fabricate biomaterials with tunable fibril nanostructure and bulk hydrogel rheological properties.

Introduction

Hydrogels are a class of materials that entrap large amounts of water and can be prepared by cross-linking polymers or by self-assembly.[1−3] Hydrogels derived from peptide self-assembly are attractive materials in this class, since structurally diverse building blocks can be obtained through facile solid-phase synthetic protocols.[4,5] Moreover, peptide materials can be rendered biologically functional by incorporating proteinaceous motifs that are known to control cellular events.[6] Thus, peptide-based gels are finding use in tissue engineering and controlled drug release applications.[7−10] Several research groups are actively designing peptides that self-assemble to afford hydrogel materials.[11−25] Preparing peptides that undergo self-assembly in response to physiologically relevant changes in their environment such as pH, temperature, ionic strength or the introduction of small molecules allows the formation of gels with temporal resolution.[4,26] Self-assembled hydrogels contain noncovalent,

‡ Department of Chemistry and Biochemistry.
† Department of Materials Science and Engineering and Delaware Biotechnology Institute.

(1) Xu, C. Y.; Kopecek, J. *Polym. Bull.* **2007**, *58*, 53−63.
(2) Goldberg, M.; Langer, R.; Jia, X. Q. *J. Biomater. Sci.-Polym. Ed.* **2007**, *18*, 241−268.
(3) Hoffman, A. S. *Adv. Drug Delivery Rev.* **2002**, *54*, 3−12.
(4) Mart, R. J.; Osborne, R. D.; Stevens, M. M.; Ulijn, R. V. *Soft Matter* **2006**, *2*, 822−835.
(5) Fairman, R.; Akerfeldt, K. S. *Curr. Opin. Struct. Biol.* **2005**, *15*, 453−463.
(6) Drury, J. L.; Mooney, D. J. *Biomaterials* **2003**, *24*, 4337−4351.
(7) Stevens, M. M.; George, J. H. *Science* **2005**, *310*, 1135−1138.
(8) Lee, K. Y.; Mooney, D. J. *Chem. Rev.* **2001**, *101*, 1869−1879.
(9) Mikos, A. G.; Herring, S. W.; Ochareon, P.; Elisseeff, J.; Lu, H. H.; Kandel, R.; Schoen, F. J.; Toner, M.; Mooney, D.; Atala, A.; Van, Dyke, M. E.; Kaplan, D.; Vunjak-Novakovic, G. *Tissue Eng.* **2006**, *12*, 3307−3339.
(10) Lutolf, M. P.; Hubbell, J. A. *Nat. Biotechnol.* **2005**, *23*, 47−55.
(11) Savin, T.; Doyle, P. S. *Soft Matter* **2007**, *3*, 1194−1202.
(12) Mahler, A.; Reches, M.; Rechter, M.; Cohen, S.; Gazit, E. *Adv. Mater.* **2006**, *18*, 1365−1370.
(13) Jayawarna, V.; Smith, A.; Gough, J. E.; Ulijn, R. V. *Biochem. Soc. Trans.* **2007**, *35*, 535−537.
(14) Wang, K.; Keasling, J. D.; Muller, S. J. *Int. J. Biol. Macromolecules* **2005**, *36*, 232−240.
(15) Collier, J. H.; Hu, B. H.; Ruberti, J. W.; Zhang, J.; Shum, P.; Thompson, D. H.; Messersmith, P. B. *J. Am. Chem. Soc.* **2001**, *123*, 9463−9464.
(16) Yang, Z.; Xu, B. *J. Mater. Chem.* **2007**, *17*, 2385−2393.
(17) Ramachandran, S.; Trewhella, J.; Tseng, Y.; Yu, Y. B. *Chem. Mater.* **2006**, *18*, 6157−6162.
(18) Schneider, J. P.; Pochan, D. J.; Ozbas, B.; Rajagopal, K.; Pakstis, L.; Kretsinger, J. *J. Am. Chem. Soc.* **2002**, *124*, 15030−15037.
(19) Zhang, S. G. *Nat. Biotechnol.* **2003**, *21*, 1171−1178.
(20) de Groot, N. S.; Parella, T.; Aviles, F. X.; Vendrell, J.; Ventura, S. *Biophys. J.* **2007**, *92*, 1732−1741.
(21) Mi, L. X.; Fischer, S.; Chung, B.; Sundelacruz, S.; Harden, J. L. *Biomacromolecules* **2006**, *7*, 38−47.
(22) Shen, W.; Zhang, K. C.; Kornfield, J. A.; Tirrell, D. A. *Nat. Mater.* **2006**, *5*, 153−158.
(23) Potekhin, S. A.; Melnik, T. N.; Popov, V.; Lanina, N. F.; Vazina, A. A.; Rigler, P.; Verdini, A. S.; Corradin, G.; Kajava, A. V. *Chem. Biol.* **2001**, *8*, 1025−1032.
(24) Ciani, B.; Hutchinson, E. G.; Sessions, R. B.; Woolfson, D. N. *J. Biol. Chem.* **2002**, *277*, 10150−10155.
(25) Dong, H.; Paramonov, S. E.; Aulisa, L.; Bakota, E. L.; Hartgerink, J. D. *J. Am. Chem. Soc.* **2007**, *129*, 12468−12472.
(26) Hartgerink, J. D.; Beniash, E.; Stupp, S. I. *Proc. Natl. Acad. Sci. U.S.A.* **2002**, *99*, 5133−5138.

physical cross-links, precluding the need for chemical cross-linkers that can be cytotoxic.[27] In addition, some physically cross-linked peptide hydrogels can immediately reheal into a solid gel after shear thinning, thereby allowing the injectible delivery of the material.[28]

In this paper, we present a peptide design where the self-assembly of secondary structural units occurs through strand-swapping, a mechanism similar to domain-swapping that is employed by some proteins to control oligomerization.[29,30] This design allows control over hydrogel nanoscale morphology and bulk material properties.

With respect to naturally occurring proteins, three-dimensional domain-swapping involves the formation of oligomeric protein quaternary structure via the exchange of common secondary structural element(s) or even globular domains between subunits.[31–33] Proteins capable of domain-swapping generally possess a loop region that separates the exchangeable domain from the remainder of the protein. A conformational change in this hinge loop region detaches the exchangeable domain from the protein fold, resulting in the formation of an open monomer. In the simplest case, two such open monomers associate to reestablish native interactions with the mutually exchanged domains, generating a natively folded, swapped dimer. Higher order oligomers such as domain-swapped trimers, tetramers, and hexamers have also been observed. Interestingly, domain-swapping has been implicated in the fibrillogenesis of human prion protein,[34] human cystatin C,[35] and β2-microglobulin.[36] Although there is debate over the exact mechanism(s) leading to fibril formation, domain-swapping propagated over a large number of open monomers is one possibility that results in higher order assemblies and aggregation.[37,38] For example, propagative domain-swapping between proteins can lead to fibril formation, where the domain of one monomer inserts into the next protein along the length of the fiber. This "runaway domain-swap" model was used to explain the fibril formation observed for T7 endonuclease and p13suc1.[30,39,40] However, propagative domain-swapping is not the only mechanism by which fibril formation can occur. Preformed, discreet, domain-swapped oligomers could also self-assemble to form amyloid-like fibrils.[41] Eisenberg and colleagues have taken advantage of this mechanism to design hybrid amyloid fibrils. A poly-glutamine cross-β spine[42]-forming sequence was inserted in the hinge loop region of ribonuclease A, a protein that undergoes domain-swapping, to guide the formation of a discreet oligomer that goes on to self-assemble.[32,41,43,44] These studies suggest that the swapping of secondary structural units can be exploited to introduce an additional level of hierarchy in the design of peptide-based, self-assembled materials.

Herein, we describe the design of a peptide-based hydrogel system whose design is inspired by domain-swapping. Peptides are designed to adopt a random coil conformation in aqueous solution at room-temperature, rendering them highly soluble. The addition of heat, which drives the hydrophobic association of side chains, triggers peptide folding and concomitant β-strand-swapping, leading to the formation of β-strand-swapped dimers (Figure 1). These dimers serve as the basic unit for self-assembly, leading to fibril formation and ultimate hydrogelation. This mechanism allows hydrogel material formation to take place with temporal resolution. Although inspired by classical domain-swapping common to proteins, our mechanism is distinct in that folded monomers do not unhinge a domain that gets swapped, resulting in oligomer formation. In contrast, β-hairpin-folding and β-strand-swapping occur simultaneously, ultimately resulting in dimers that self-assemble. Hairpin-folding, swapping, and self-assembly are most likely linked equilibria. Strand-swapping is used as a positive design element to control self-assembly events that govern nanoscale fibril morphology and macroscale bulk rheological properties.

Results and Discussion

Peptide Design. Although hairpin-folding, strand-swapping, and oligomer self-assembly are most likely linked processes, it is convenient to discuss the design of this hydrogelation system as if these events occurred sequentially. Under folding solution conditions, strand-swapping peptide 1 (SSP1) was designed to adopt a β-hairpin that displays an exchangeable β-strand region. This strand region operates as an exchangeable domain (blue ribbon in Figure 1) that can participate in swapping with the exchangeable β-strand of another peptide. This results in the formation of a β-strand-swapped dimer, which constitutes a two-stranded antiparallel, amphiphilic sheet that is highly prone to self-assemble. Self-assembly is designed to take place facially, where two dimeric sheets associate to bury their hydrophobic faces from water, forming a bilayer. In addition, the dimeric unit is designed to self-assemble laterally, forming hydrogen bonds along the length of the fibril. Figure 1 shows an expanded view of the fibril formed from SSP1. A simplified stick representation of the peptide is used to show the strand-swapped β-sheet assembly along the hydrogen-bonding axis of the fibril. Here, the fibril is composed of a bilayer of hydrogen-bonded, strand-swapped dimers.

Although many types of secondary and globular structures can serve as exchangeable domains, a β-strand was incorporated into SSP1. This choice was based on the observation that most proteins that use strands for swapping ultimately form discreet dimers, as opposed to higher order oligomers.[35,45–51] The

(27) Hennink, W. E.; van Nostrum, C. F. *Adv. Drug Delivery Rev.* **2002**, *54*, 13–36.
(28) Haines-Butterick, L.; Rajagopal, K.; Branco, M.; Salick, D.; Rughani, R.; Pilarz, M.; Lamm, M. S.; Pochan, D. J.; Schneider, J. P. *Proc. Natl. Acad. Sci. U.S.A.* **2007**, *104*, 7791–7796.
(29) Bennett, M. J.; Choe, S.; Eisenberg, D. *Proc. Natl. Acad. Sci. U.S.A.* **1994**, *91*, 3127–3131.
(30) Bennett, M. J.; Schlunegger, M. P.; Eisenberg, D. *Protein Sci.* **1995**, *4*, 2455–2468.
(31) Rousseau, F.; Schymkowitz, J. W. H.; Itzhaki, L. S. *Structure* **2003**, *11*, 243–251.
(32) Liu, Y.; Eisenberg, D. *Protein Sci.* **2002**, *11*, 1285–1299.
(33) Newcomer, M. E. *Curr. Opin. Struct. Biol.* **2002**, *12*, 48–53.
(34) Knaus, K. J.; Morillas, M.; Swietnicki, W.; Malone, M.; Surewicz, W. K.; Yee, V. C. *Nat. Struct. Biol.* **2001**, *8*, 770–774.
(35) Janowski, R.; Kozak, M.; Jankowska, E.; Grzonka, Z.; Grubb, A.; Abrahamson, M.; Jaskolski, M. *Nat. Struct. Biol.* **2001**, *8*, 316–320.
(36) Eakin, C. M.; Attenello, F. J.; Morgan, C. J.; Miranker, A. D. *Biochemistry* **2004**, *43*, 7808–7815.
(37) Newcomer, M. E. *Nat. Struct. Biol.* **2001**, *8*, 282–284.
(38) Sinha, N.; Tsai, C. J.; Nussinov, R. *Protein Eng.* **2001**, *14*, 93–103.
(39) Guo, Z. F.; Eisenberg, D. *Proc. Natl. Acad. Sci. U.S.A.* **2006**, *103*, 8042–8047.
(40) Rousseau, F.; Wilkinson, H.; Villanueva, J.; Serrano, L.; Schymkowitz, J. W. H.; Itzhaki, L. S. *J. Mol. Biol.* **2006**, *363*, 496–505.
(41) Bennett, M. J.; Sawaya, M. R.; Eisenberg, D. *Structure* **2006**, *14*, 811–824.
(42) Nelson, R.; Sawaya, M. R.; Balbirnie, M.; Madsen, A. O.; Riekel, C.; Grothe, R.; Eisenberg, D. *Nature* **2005**, *435*, 773–778.
(43) Nelson, R.; Eisenberg, D. *Curr. Opin. Struct. Biol.* **2006**, *16*, 260–265.
(44) Sambashivan, S.; Liu, Y. S.; Sawaya, M. R.; Gingery, M.; Eisenberg, D. *Nature* **2005**, *437*, 266–269.
(45) Spinelli, S.; Desmyter, A.; Frenken, L.; Verrips, T.; Tegoni, M.; Cambillau, C. *FEBS Lett.* **2004**, *564*, 35–40.
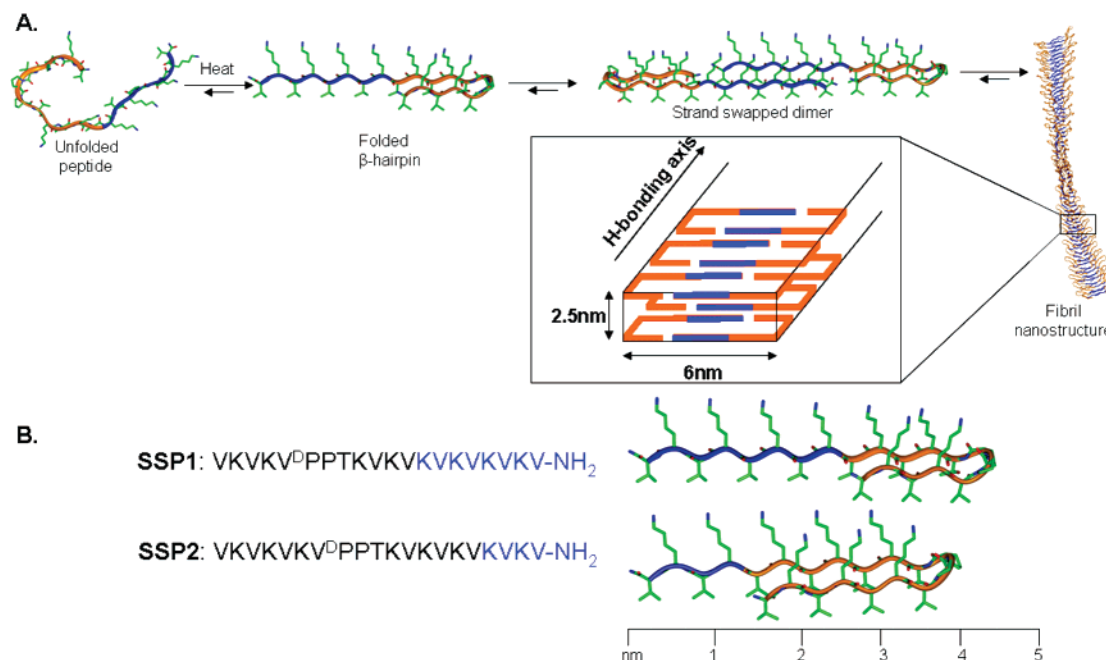
Figure 1. (A) Schematic of the proposed self-assembly mechanism for strand-swapping peptide (SSP1). (B) Sequences of SSP1 and SSP2 with corresponding β-hairpin illustrations. The exchangeable domains of SSP1 and SSP2 are 2.8 and 1.4 nm in length, respectively.
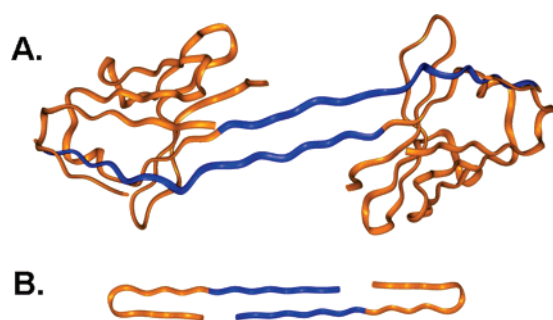

Figure 2. (A) Domain-swapped dimer of VHH-R9 (PDB entry 1SJV). (B) β-Strand-swapped dimer of SSP1. The exchangeable domains are shown in blue and the nonexchangeable domains are shown in orange.

structure of llama antibody VHH-R9, a domain-swapped dimer, provides a beautiful example (Figure 2A).[45] This protein contains an 11-residue exchangeable β-strand that hydrogen bonds with the corresponding strand of the second subunit. This results in the formation of a highly regular two-stranded antiparallel β-sheet that connects the two globular domains. Since our self-assembly strategy necessitates the formation of swapped dimers, the β-strand presented itself as the ideal motif for use as the exchangeable domain (Figure 2B, blue portion). SSP1 contains an exchangeable strand composed of eight residues. Its length was based on our assessment of reported protein strand-swapped dimers, which included nine proteins, namely, Cks1,[50] Trk-D5,[49] MARCO,[48] dynein light chain DLC8b,[47] VHH-R9,[45] p13suc1,[51]

nitric oxide synthase,[52] human cystatin C,[35] and mutant GB1 HS#124F26A;[46] typically, strand lengths of 4−11 residues are observed. In a second design, SSP2, the length of the exchangeable strand was decreased to four residues to assess the influence that length has on self-assembly, fibril morphology, and ultimate hydrogel material properties.

The nonexchangeable domains of the SSP peptides are simple β-hairpin motifs. In swapped-protein oligomers, nonexchangeable domains primarily consist of globular structures[31,32] (Figure 2A, orange portion). Designing globular domains de novo is challenging, especially for self-assembling systems in which extensive intermolecular interactions formed during assembly must be taken into account. Thus, the less complex β-hairpin structural unit is used as the nonexchangeable domain of the SSP peptides (Figure 2B). The hairpin scaffold not only serves to display the exchangeable strand domain for swapping but also provides hydrogen-bond donors and acceptors, relatively simple interactions to design, to propagate self-assembly.

These design considerations resulted in two peptides, SSP1 and SSP2, which are themselves β-hairpins that simply contain asymmetric strands (Figure 1). The strand regions are composed of an alternating sequence of hydrophilic lysine and hydrophobic valine residues flanking a β-turn. The C-terminal strand is amidated and the N-terminal strand presents a free amine. When these peptides fold and dimerize, this sequential arrangement in the strand regions provides amphiphilicity to the faces of the strand-swapped dimer. This ultimately allows the dimer to self-assemble facially, burying its valine-rich face to form a bilayer. Although the mechanism in Figure 1A implies the initial formation of the hairpin that goes on to dimerize, there is no experimental evidence that this is the case. Unfolded peptide could directly afford a dimer if folding and self-assembly were concurrent events. Distinguishing between the two mechanisms

(46) Byeon, I. J. L.; Louis, J. M.; Gronenborn, A. M. *J. Mol. Biol.* **2003**, *333*, 141−152.
(47) Wang, W. N.; Lo, K. W. H.; Kan, H. M.; Fan, J. S.; Zhang, M. J. *J. Biol. Chem.* **2003**, *278*, 41491−41499.
(48) Ojala, J. R. M.; Pikkarainen, T.; Tuuttila, A.; Sandalova, T.; Tryggvason, K. *J. Biol. Chem.* **2007**, *282*, 16654−16666.
(49) Ultsch, M. H.; Wiesmann, C.; Simmons, L. C.; Henrich, J.; Yang, M.; Reilly, D.; Bass, S. H.; de Vos, A. M. *J. Mol. Biol.* **1999**, *290*, 149−159.
(50) Seeliger, M. A.; Spichty, M.; Kelly, S. E.; Bycroft, M.; Freund, S. M. V.; Karplus, M.; Itzhaki, L. S. *J. Biol. Chem.* **2005**, *280*, 30448−30459.
(51) Schymkowitz, J. W. H.; Rousseau, F.; Itzhaki, L. S. *J. Mol. Biol.* **2000**, *301*, 199−204.

(52) Crane, B. R.; Rosenfeld, R. J.; Arvai, A. S.; Ghosh, D. K.; Ghosh, S.; Tainer, J. A.; Stuehr, D. J.; Getzoff, E. D. *EMBO J.* **1999**, *18*, 6271− 6281.

is extremely difficult. In Figure 1, the simplest mechanism possible is shown.

In the SSP1 and SSP2 peptides, valines were incorporated at non-hydrogen-bonding positions in the strand regions to promote intermolecular van der Waal contacts with the valines of neighboring peptides in the self-assembled fibril.[53,54] The turn region consists of the tetrapeptide sequence $(-V^{D}PPT-)$ designed to adopt a type II′ turn, a geometry commonly found in β-hairpin motifs of naturally occurring proteins.[55-59] The threonine residue at the $i + 3$ position of the turn was included, since it has a high propensity to occupy this position in type II′ turns of hairpins found in naturally occurring proteins.[60] Threonine can form a stabilizing side chain−main chain H-bond between its alcoholic proton and the carbonyl oxygen of the ith residue of the turn.

These peptides are designed to undergo triggered folding and self-assembly to allow material formation to take place in response to heat. When the peptides are dissolved in aqueous solution at pH 9.0, some of the lysine side chains are deprotonated, which poises the peptide to fold. However, at ambient temperatures, water is capable of solvating the hydrophobic portions of the peptides, rendering them soluble. When the temperature is raised, the hydrophobic effect dominates and the peptides fold and assemble to bury their hydrophobic regions. Self-assembly leads to a fibrillar network that traps large amounts of water to form self-supporting three-dimensional hydrogels.

Triggered Peptide Folding and Self-Assembly. Figure 3 shows circular dichroism (CD) spectra of SSP1 and SSP2, where the mean residue ellipticity at 216 nm, which is indicative of β-sheet structure, is measured as a function of temperature. Spectra were obtained at a peptide concentration of 150 μM, which does not provide enough peptide to gel the buffer solution. However, under these dilute concentrations, the peptide still folds and assembles, forming structures that are sufficiently small so that they do not appreciably scatter light. This enables spectroscopic measurements of secondary structure formation.

Figure 3A shows that, at pH 9.0, both SSP1 and SSP2 are unfolded at temperatures less than 35 °C. However, increasing the temperature to 37 °C initiates folding and assembly, and at 50 °C, the transition is complete. Figure 3B shows wavelength spectra of the peptides at 15 °C that are indicative of random coil structure. Spectra obtained at 50 °C are consistent with β-sheet structure, having minima centered at about 216 nm and maxima at 195 nm. Since temperature-dependent folding and assembly are largely driven by the hydrophobic effect[61,62] for these peptides, it is expected that both SSP1 and SSP2 fold and assemble at about the same temperature, since their amino acid composition and the spatial arrangement of their hydrophobic
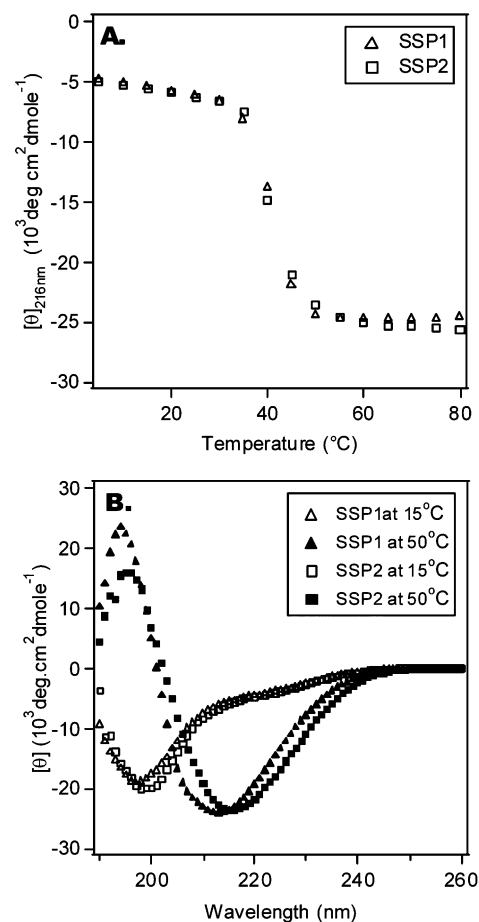

Figure 3. CD spectra of SSP1 and SSP2 (150 μM peptide at pH 9, 125 mM borate, 10 mM NaCl). (A) β-sheet formation monitored at $[\theta]_{216nm}$ as a function of temperature. (B) Wavelength CD spectra of SSP1 and SSP2 at 15 and 50 °C.

side chains are similar. The transition from random coil to β-sheet is irreversible for both peptides. The formation of β-sheet secondary structure in the self-assembled state was also observed at a peptide concentration that results in gelation by Fourier transform infrared spectroscopy (FTIR) (see the Supporting Information, Figure S3). FTIR spectra of 1 wt % SSP1 and SSP2 hydrogels prepared at pH 9.0 and 50 °C showed amide I′ stretches centered at 1616 cm^{-1} for both peptide gels, indicative of β-sheet structure. A small stretch at 1680 cm^{-1} was also observed and may be attributed to the proposed antiparallel nature of the self-assembly.[63] The β-sheet secondary structural content of both SSP1 and SSP2 1 wt % gels was also verified by wide-angle X-ray scattering (WAXS). Diffraction peaks that yield d-spacing of 4.7 Å, corresponding to the interstrand hydrogen-bonding repeat,[42,64] were observed (see the Supporting Information, Figure S-4). Taken together, these data indicate that both SSP1 and SSP2 undergo thermally triggered folding and self-assembly to afford β-sheet-rich hydrogels.

Nanostructure of SSP1 Hydrogels. The nanostructure of the network that defines the SSP1 gel was investigated using a combination of transmission electron microscopy (TEM), small angle neutron scattering (SANS), and atomic force microscopy (AFM). Figure 4A shows a negatively stained bright-field image

(53) Rajagopal, K.; Ozbas, B.; Pochan, D. J.; Schneider, J. P. *Eur. Biophys. J. Biophys. Lett.* **2006**, *35*, 162−169.
(54) Wouters, M. A.; Curmi, P. M. G. *Proteins*−Struct. Funct. Genet. **1995**, *22*, 119−131.
(55) Sibanda, B. L.; Thornton, J. M. *Nature* **1985**, *316*, 170−174.
(56) Nair, C. M.; Vijayan, M.; Venkatachalapathi, Y. V.; Balaram, P. *J. Chem. Soc. Chem. Commun.* **1979**, 1183−1184.
(57) Gunasekaran, K.; Ramakrishnan, C.; Balaram, P. *Protein Eng.* **1997**, *10*, 1131−1141.
(58) Chalmers, D. K.; Marshall, G. R. *J. Am. Chem. Soc.* **1995**, *117*, 5927−5937.
(59) Favre, M.; Moehle, K.; Jiang, L. Y.; Pfeiffer, B.; Robinson, J. A. *J. Am. Chem. Soc.* **1999**, *121*, 2679−2685.
(60) Hutchinson, E. G.; Thornton, J. M. *Protein Sci.* **1994**, *3*, 2207−2216.
(61) Makhatadze, G. I.; Privalov, P. L. *J. Mol. Biol.* **1993**, *232*, 639−659.
(62) Privalov, P. L.; Makhatadze, G. I. *J. Mol. Biol.* **1993**, *232*, 660−679.

(63) Kubelka, J.; Keiderling, T. A. *J. Am. Chem. Soc.* **2001**, *123*, 12048−12058.
(64) Makin, O. S.; Atkins, E.; Sikorski, P.; Johansson, J.; Serpell, L. C. *Proc. Natl. Acad. Sci. U.S.A.* **2005**, *102*, 315−320.
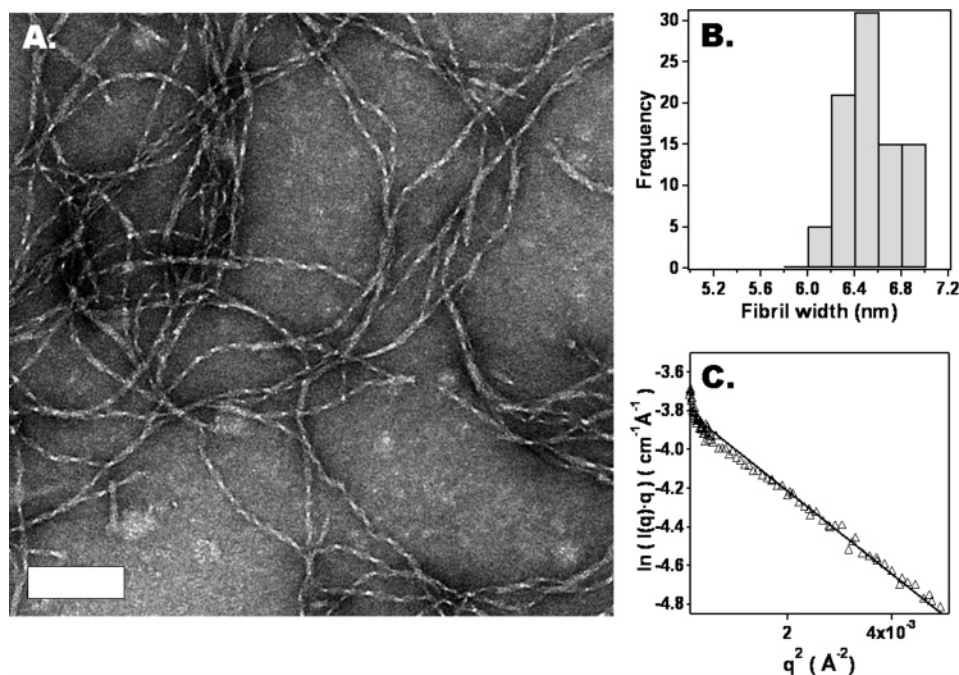
Figure 4. (A) TEM displaying the twisted fibril nanostructure of SSP1. Scale bar = 100 nm. (B) The histogram of multiple width measurements ($N = 83$) provided an average fibril width of 6.4 nm. (C) SANS modified Guinier analysis of SSP1 fibrils obtained from a 1 wt % SSP1 hydrogel (pH 9, 125 mM borate, 10 mM NaCl, 20 °C, D_2O) indicating a rod diameter of 5.9 nm (58.5 Å).

of the local nanostructure that defines the SSP1 gel. SSP1 forms fibrils that have a regular, repeated twist, as evidenced from the alternating light and dark bands observed on fibrils in the micrograph. The fibrils are monodisperse in width but have varying lengths, often several microns. Fibril width, a measurement perpendicular to the long axis of the fibril lying on the grid surface, was quantified by taking a statistically significant number of measurements ($N = 83$) of different fibrils from several independent high-resolution images (Figure 4B). SSP1 fibrils are 6.4 ± 0.2 nm in width as observed by TEM.

No other fibril morphologies were observed by TEM, suggesting that SSP1 self-assembles in a highly regular manner. However, TEM only provides structural information for a small percentage of the total number of fibrils that define the gel. SANS was used to globally measure the average width of the SSP1 fibrils that constitute the gel. A modified Guinier analysis of a 1 wt % SSP1 hydrogel in D_2O is shown in Figure 4C. Assuming fibrils behave as rodlike particles, a plot of $\ln[I(q)q]$ versus q^2 yields a slope that is equal to $-R_c^2/2$, where $I(q)$ is the scattering intensity as a function of the scattering vector q and R_c is the cross-sectional radius of gyration for the rodlike particle.[65-67] The scattering vector q is defined as $q = (4\pi/\lambda)\sin(\theta/2)$, where λ is the neutron beam wavelength and θ is the scattering angle. The radius of a SSP1 fibril is given by $R = R_c\sqrt{2}$. This analysis provides an average radius of 29.3 Å, which corresponds to a fibril diameter of 5.9 nm (58.6 ± 0.2 Å), close to that measured by TEM. These independent measurements of fibril width are consistent with the proposed model of self-assembly for SSP1 where the

formation of the β-strand-swapped dimer defines this dimension. Specifically, the fibril width is defined by the sum of the lengths of the short N-terminal β-strand of one hairpin and the longer C-terminal β-strand of the second hairpin containing the exchangeable domain (Figure 1).

The TEM data in Figure 4A shows that the SSP1 fibrils are twisted. Sixty-three independent measurements of pitch provide a value of 50.4 ± 5.8 nm. This suggests that there are about 27 domain-swapped dimers in every helical repeat. The fibril twist observed by TEM is also supported by AFM measurements of fibril height. If the fibrils were nontwisting, their height would be defined by the bilayer formed by the facial self-assembly of two domain-swapped dimers, namely, 2.5 nm. However, if the fibrils are twisted, the height will be equal to the width and defined by the sum of the lengths of the short N-terminal β-strand of one hairpin and the longer C-terminal β-strand of the second hairpin, as discussed above. Figure 5A shows a pictorial representation of a twisted fibril lying flat on a surface. The domain-swapped assembly of SSP1 hairpins is also shown along the long axis of the fibril.

Figure 5B shows a representative tapping mode height image of SSP1 fibrils. The twisted fibril morphology is clearly evidenced by the presence of a beaded structure. The bright and dark areas correspond to consecutive increases and decreases in the height, respectively, as the bilayer of domain-swapped dimers traverses about the central fibril axis. Such regular and repeated variations in height correlate well with a twisted morphology. Fibril height was quantitatively determined via 47 independent measurements (Figure 5C), which result in a mean height of 6.0 ± 0.3 nm, in agreement with the domain-swapped fibril model.

Spectroscopy, microscopy, and scattering data suggests that SSP1 undergoes β-strand-swapping to form discreet dimers that constitute the basic unit of self-assembly. Strand-swapped dimers

(65) Burkoth, T. S.; Benzinger, T. L. S.; Urban, V.; Morgan, D. M.; Gregory, D. M.; Thiyagarajan, P.; Botto, R. E.; Meredith, S. C.; Lynn, D. G. *J. Am. Chem. Soc.* **2000**, *122*, 7883−7889.
(66) Guinier, A.; Fournet, G. *Small-Angle Scattering of X-rays;* Wiley-Interscience: New York, 1955.
(67) Ozbas, B.; Rajagopal, K.; Schneider, J. P.; Pochan, D. J. *Phys. Rev. Lett.* **2004**, *93*.
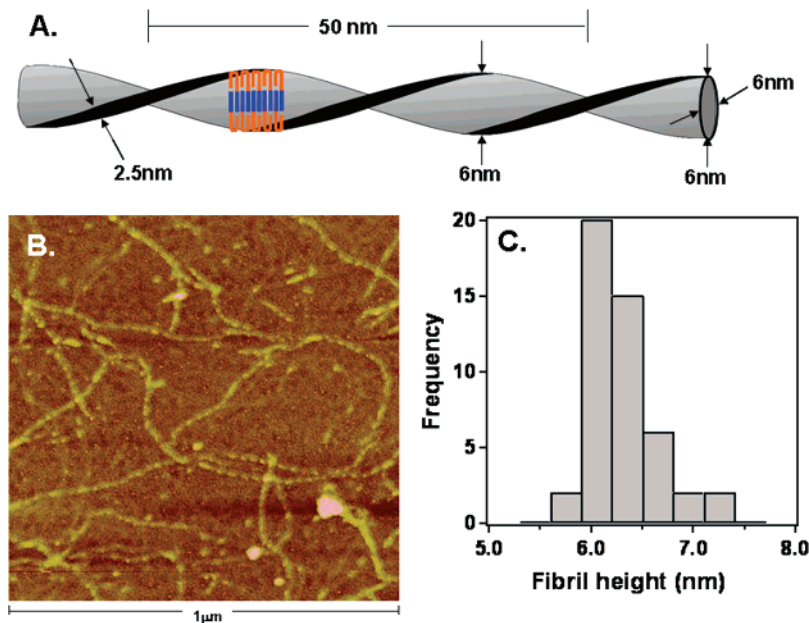
Figure 5. (A) Illustration of the twisted ribbon fibril morphology of SSP1 based on TEM, SANS, and AFM. Representative strand-swapped peptide assembly (shown in blue and orange) is depicted along the fibril, which is shown lying flat on a surface and viewed from the top. Bilayer formation is not depicted in this scheme for clarity. (B) Tapping mode AFM measurements of the fibrils in topology mode. A $1 \times 1 \ \mu$m image is shown. The alternate dark and bright bands on the SSP1 fibrils indicate a periodic twist. (C) Multiple fibril height measurements ($N = 47$) provide an average height of 6.0 nm with the frequency distribution shown.

self-assemble laterally via H-bond formation along the fibril long axis. Although it is difficult to directly observe bilayer formation in twisted fibrils, modeling suggests that the strand-swapped dimers also assemble facially, burying their hydrophobic faces from water. This is a reasonable assumption given that SSP2, a peptide of similar sequence composition, assembles into nontwisting fibrils, where bilayer formation is directly observed (vide infra). Concerning the exact mechanism of self-assembly, there is no direct evidence that indicates that domain-swapped dimers are formed first and that these dimers go onto assemble. Again, intramolecular peptide-folding, domain-swapping, and self-assembly are most likely linked processes, occurring simultaneously.

Nanostructure of SSP-2 Hydrogels: Effect of Modulating the Length of the Exchangeable Domain. SSP1 contains an exchangeable β-strand domain of eight residues, the median number of residues typically found in proteins that use this motif for swapping. SSP2 contains four residues in its exchangeable domain, the minimal number of residues typically used. Using a small exchangeable domain tests the limits of strand-swapping as a tool in self-assembly. Instead of swapping its β-strand to form a dimer that serves as the constitutive unit of assembly, monomers of SSP2 could simply hydrogen bond repetitively along the long axis of the fibril. Here, eight hydrogen-bond donors and acceptors would go unfulfilled. Although not an energetically optimal H-bonding pattern, it could still occur.

Figure 6A shows a TEM micrograph of fibrils formed by the self-assembly of SSP2. The fibril width assessed from multiple TEM ($N = 79$) measurements provides an average width of 6.2 ± 0.3 nm (Figure 6B). The width is consistent with the formation of a strand-swapped dimer. If monomers of SSP2 were serving as the repetitive unit of assembly, the fibril width would be on the order of about 4 nm (Figure 1B). This width value is clearly outside the range measured by TEM. A modified Guinier analysis of SANS data collected from a SSP2

hydrogel provides an approximate fibril diameter of 6.2 nm (61.5 ± 0.2 Å), which is in good agreement with the TEM data and further supports the formation of a swapped dimer. This data suggests that forgoing the formation of eight hydrogen bonds provides enough of an energetic barrier to disfavor monomer assembly and that short exchangeable domains can operate effectively to guide self-assembly.

However, although swapping still occurs, the size of the exchangeable domain does directly influence the morphology of the fibrils that are formed. The TEM micrograph in Figure 6A shows that SSP2 forms fibrils that are untwisted. This untwisted morphology presents an opportunity to experimentally observe bilayer formation for SSP2 fibrils. This was not possible for the twisting SSP1 fibrils. AFM measurement of fibril height provides experimental verification that bilayer formation is occurring. Figure 7B shows a representative AFM micrograph of SSP2 fibrils showing a nontwisted morphology. Importantly, independent height measurements ($N = 115$) were taken at distinct fibril locations to produce the histogram shown in Figure 7C. The measured, average fibril height of 2.5 ± 0.2 nm is consistent with the formation of a bilayer formed from the facial association of strand-swapped dimers. The microscopy and scattering data support the model of assembly depicted in Figure 7A, where β-strand-swapped dimers hydrogen bond along the fibril long axis and facially associate to form a bilayer that defines the fibril height.

Bulk Rheological Material Properties. Both SSP1 and SSP2 self-assemble to form viscoelastic hydrogels. The effect of modulating the size of the exchangeable domain on the viscoelastic properties, kinetics of network formation, and rigidity of the hydrogel were assessed by oscillatory shear rheology. Figure 8 shows dynamic time sweep data that measures the evolution of storage modulus (G'), a measure of the material's elastic response to stress, i.e., rigidity, as a function of time. In this experiment, a 2 wt % solution of either
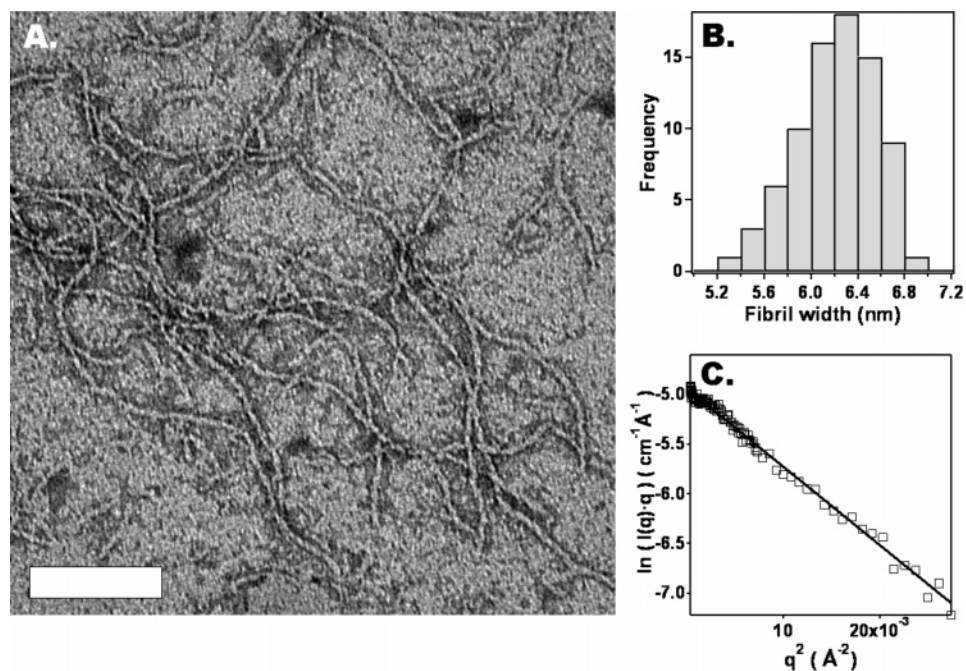
Figure 6. (A) TEM displaying the untwisted fibril nanostructure of SSP2. Scale bar = 100 nm. (B) The histogram of multiple fibril width measurements (N = 79) provided an average width of 6.2 nm. (C) SANS modified Guinier analysis of SSP2 fibrils obtained from a 1 wt % SSP2 hydrogel (pH 9, 125 mM borate, 10 mM NaCl, 20 °C, D_2O) indicating a rod diameter of 6.2 nm (61.5 Å).
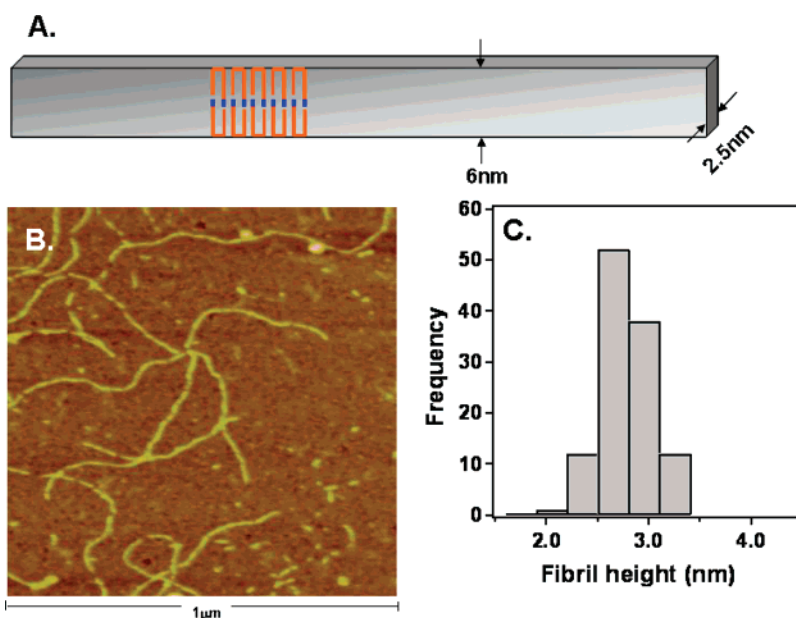

Figure 7. (A) Illustration of the untwisted fibril morphology of SSP2 based on TEM, SANS, and AFM. Representative β-strand-swapped peptide assembly (blue and orange) is depicted along the fibril, which is shown lying flat on a surface and viewed from the top. Bilayer formation is not shown in this scheme for clarity. (B) Tapping mode AFM measurements of the fibrils in topology mode. A $1 \times 1 \mu$m image is shown. (C) Multiple height measurements (N = 115) provide an average fibril height of 2.5 nm with the frequency distribution shown.

unfolded SSP1 or SSP2 is heated to 50 °C to initiate folding, strand-swapping, and self-assembly. After 1 h, self-assembly leading to hydrogelation is complete, affording gels with G' of 367 ± 23 and 517 ± 40 Pa for SSP1 and SSP2, respectively. The small, time-dependent increase in G' at longer times (greater than 30 min) is most likely due to small changes in the gel's network structure that positively influences G'. This data also shows that SSP2 forms hydrogel materials at a faster rate than SSP1. Figure 8B shows frequency sweep data that measures the storage modulus (G') and the loss modulus (G'', a measure of the material viscous response to stress) as a function of

frequency. It can be seen that the values of G' are an order of magnitude greater than G'' for both SSP1 and SSP2 gels. Also, there is no crossover observed for the values of G' and G'' in the large frequency range investigated (0.1–100 rad/s), and G' is insensitive to frequency for both peptide gels. Taken together, these data suggest that both SSP1 and SSP2 form mechanically rigid gels, demonstrating solidlike behavior.[67-69] The varying

(68) Mackintosh, F. C.; Kas, J.; Janmey, P. A. *Phys. Rev. Lett.* **1995**, *75*, 4425–4428.
(69) Kavanagh, G. M.; Ross-Murphy, S. B. *Prog. Polym. Sci.* **1998**, *23*, 533–562.
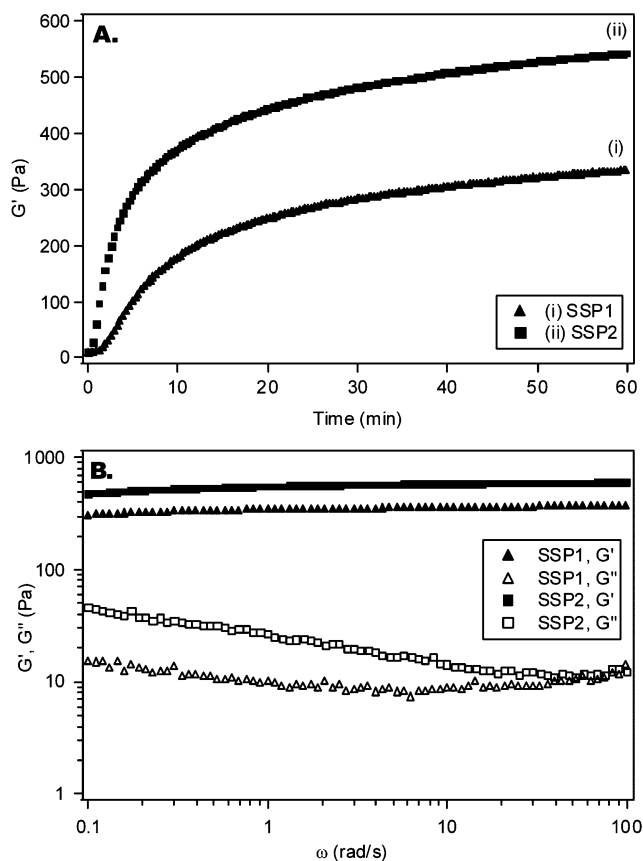
Figure 8. Oscillatory rheology of 2 wt % peptide hydrogels (0.2% strain, angular frequency = 6 rad s^{-1}, 50 °C, pH 9, 125 mM borate, 10 mM NaCl). (A) Dynamic time sweeps show the evolution of the storage modulus (G') as a function of time. (B) Dynamic frequency sweeps showing the dependence of G' and G'' (loss modulus) from 0.1 to 100 rad s^{-1} of SSP1 and SSP2 hydrogels.

biomedical applications that employ hydrogel materials call for gels of differing rigidities, depending on the application at hand. For example, in tissue regenerative applications where gels are introduced to wound sites, matching hydrogel mechanical properties with that of the target tissue is important.[70] The data in Figure 8 demonstrate that strand-swapping may be a useful tool for formulating materials with prerequisite mechanical properties.

The differences in the bulk rheological properties of SSP1 and SSP2 gels are manifested through differences in the fibril network structure that defines each gel. This, in turn, is dependent on fibril morphology. The twisted versus nontwisted morphologies of SSP1 and SSP2 fibrils can be attributed to the variable length of the exchangeable domains and its influence on self-assembly. A molecular level explanation for these morphological differences would be speculative without high-resolution structural data. However, the degree of intrinsic strand twist,[54,71–74] which would vary in strand domains of different lengths, may help define fibril morphology.

(70) Bhat, S. V. *Biomaterials*; Springer: New York, 2002.
(71) Aggeli, A.; Nyrkova, I. A.; Bell, M.; Harding, R.; Carrick, L.; McLeish, T. C. B.; Semenov, A. N.; Boden, N. *Proc. Natl. Acad. Sci. U.S.A.* **2001**, *98*, 11857–11862.
(72) Chou, K. C.; Scheraga, H. A. *Proc. Natl. Acad. Sci. U.S.A.*—Phys. Sci. **1982**, *79*, 7047–7051.
(73) Chothia, C. *J. Mol. Biol.* **1973**, *75*, 295–302.
(74) Richardson, J. S. *Adv. Protein Chem.* **1981**, *34*, 167–339.

Conclusions

Two peptides have been designed that undergo thermally triggered folding, β-strand-swapping, and self-assembly to afford mechanically rigid hydrogels composed of β-sheet-rich fibrils. SSP1 is a 20-residue peptide that, at room temperature, adopts an ensemble of random coil conformations, rendering it highly soluble in aqueous solution. When the temperature is elevated, it adopts a hairpin conformation that displays an exchangeable β-strand domain composed of eight residues. Strand-swapping between two distinct peptides affords a domain-swapped dimer that serves as the basic unit of assembly in fibril formation. SSP1 self-assembles into twisted fibrils that are 6.4 nm in width, 6.0 nm in height, and have a pitch of 50.4 nm. These dimensions are consistent with the formation of β-strand-swapped dimers that have self-assembled laterally via H-bond formation along the long axis of the fibril and facially to form a bilayer. Approximately 27 domain-swapped dimers twist around the central fibril axis to define its helical repeat. SSP2 contains an exchangeable strand domain of only four residues. Data indicate that this peptide is also capable of β-strand-swapping, forming dimers that serve as the basic unit of fibril assembly. In a similar manner to SSP1, SSP2 assembles both facially to form a bilayer and laterally, forming hydrogen bonds along the fibril long axis. However, SSP2 fibrils have a distinct nontwisted morphology. Oscillatory rheology demonstrates that differences in fibril morphology influence the bulk mechanical properties of the hydrogels formed by these peptides. This demonstrates that β-strand-swapping, a process similar to domain-swapping in natural proteins, may be a useful tool to control the nanoscale structure of materials to effect changes in their bulk properties.

Experimental Section

Materials. Trifluoroacetic acid (TFA), thioanisole, anisole, ethanedithiol, *N,N*-diisopropylethylamine, boric acid, and D$_2$O were purchased from Acros Organics. Piperidine, 1,8-diazabicyclo[5.4.0]undec-7-ene (DBU) were purchased from Aldrich. Acetic anhydride and *N*-methylpyrrolidone were obtained from EMD Biosciences. Appropriately side chain protected Fmoc amino acids were acquired from Novabiochem. HCTU coupling reagent, i.e., 1*H*-benzotriazolium 1-[bis(dimethylamino)methylene]-5-chlorohexafluorophosphate (1-)3-oxide was obtained from Peptides International. Rink amide resin was purchased from Polymer Laboratories. All peptides were purified using a Vydac semipreparative C18 peptide/protein column, and HPLC solvents used were solvent A (0.1% TFA in water) and solvent B (90% acetonitrile, 10% water, and 0.1% TFA).

Peptide Synthesis. Peptides were prepared on an automated solid-phase peptide synthesizer (ABI 433A) employing standard Fmoc chemistry protocols. Synthesis was carried out on a rink amide resin support using HCTU activation chemistry, while 1% DBU, 19% piperidine in NMP was employed to afford the Fmoc-deprotection. Following solid-phase synthesis, the peptide was cleaved off the support as well as side chain deprotected by stirring the resin-bound peptide in a cocktail containing 90:5:3:2 TFA:thioanisole:ethanedithiol:anisole under a N$_2$ atmosphere for 2 h. The resin was removed by filtration and the peptide was precipitated with cold ether to yield crude peptide that was subsequently purified using semipreparatory reverse-phase HPLC (Waters 600 series). Purification by reverse-phase HPLC for SSP1 employed a linear gradient from 0 to 20% solvent B over 20 min followed by a linear gradient from 20 to 100% B in 320 min. SSP1 eluted after 45 min using the aforementioned solvent gradient. SSP2 was purified using isocratic conditions at 0% B for 2 min followed by a linear gradient from 0 to 25% B in 2 min and a linear gradient from 0 to 25% B in 25 min followed by an additional linear gradient

from 25 to 100% B in 150 min. Using this gradient, SSP2 eluted from the C18 column with a retention time of 36 min. The purified peptides from HPLC were lyophilized to a white powder. The purity of the peptides was assessed by using analytical reverse phase HPLC (Agilent, HP 1100 series analytical HPLC) as well as electrospray ionization mass spectrometry (ESI-MS) on a Thermo Finnigan LCQ mass spectrometer. The calculated molecular weights for SSP1 and SSP2 are identical: $[M + 2H]^{2+} = 1115.9$; observed $[M + 2H]^{2+}$, SSP1, 1115.4; SSP2, 1115.7. Representative HPLC traces and MS of the peptides can be found in the Supporting Information (see Figures S-1 and S-2).

Preparation of Hydrogels. Homogeneous, optically clear gels were obtained using a procedure described below that affords a 1 wt % hydrogel. A 2 wt % peptide stock was prepared by dissolving 10 mg of lyophilized peptide in 500 μL of deionized water. The 2 wt % stock was mixed in a 1:1 ratio with 500 μL of buffer (pH 9, 250 mM borate, 20 mM NaCl) to yield 1 wt % peptide with 125 mM borate and 10 mM NaCl at pH 9. This solution was heated at 50 °C for 15 min to afford a hydrogel.

Circular Dichroism Spectroscopy. All measurements were carried out on a Jasco J-810 spectropolarimeter using a 0.1 cm path length quartz cell. Spectra were recorded for a peptide concentration of 150 μM in pH 9 buffer containing 125 mM borate and 10 mM NaCl. Sample concentrations were determined by UV absorbance employing a molar extinction coefficient of $\epsilon_{220nm} = 15\,750$ cm^{-1} M^{-1} for both peptides. A typical experiment involved equilibrating aqueous solutions of 300 μM peptide stock and pH 9 buffer (250 mM borate, 20 mM NaCl) at 5 °C prior to mixing the two solutions in a 1:1 ratio in the quartz cell, also pre-equilibrated at 5 °C. Wavelength spectra from 260 to 190 nm were recorded at temperatures of 5−80 °C with 5 °C intervals and an equilibration time of 10 min at each temperature. Appropriate blanks containing buffer concentrations identical to that used in the experiment were subtracted from each dataset. Raw data in terms of the observed ellipticity (θ_{obs}) were recorded at a dynode voltage below 500 V and converted to mean residue ellipticity $[\theta]$ by the formula $[\theta] = (\theta_{obs}/10clr)$ where c is the molar concentration of the peptide, l is the cell path length, and r is the number of residues in the peptide sequence.

Rheology. Rheological measurements were carried out on a TA instruments AR 2000 controlled-stress rheometer equipped with 25 mm stainless steel parallel plate geometry. A gap of 500 μm and a temperature of 50 °C were used for all experiments. The temperature of 50 °C is well above the thermal transition temperature measured by CD and facilitates hydrogelation on the rheometer plate. For the dynamic time sweep experiments, the rheometer was equilibrated at 5 °C prior to sample loading. Hydrogel (300 μL of 2 wt %) (formed immediately after mixing an aqueous peptide stock with an equal volume of buffer at 5 °C) was loaded on the rheometer. S3 viscosity standard mineral oil (viscosity at 50 °C = 2.028 mPa·s) was placed around the sample to prevent evaporation at high temperatures. Sample loading was followed by a temperature ramp from 5 to 50 °C at a rate of 30 °C/min. Time sweep data was collected at a constant temperature of 50 °C for 1 h with an angular frequency of 6 rad/s and a strain of 0.2%. Time sweep experiments were immediately followed by frequency sweep (0.1−100 rad/s, 0.2% strain, 50 °C) and strain sweep experiments (0.01−100% strain, angular frequency 6 rad/s, 50 °C). All reported values of G' are a mean of three discrete measurements on three different samples exhibiting a standard deviation of less than 10%.

Transmission Electron Microscopy. Bright-field images of diluted hydrogel samples were obtained using a FEI Technai-12 transmission electron microscope at an accelerating voltage of 120 kV with a Gatan CCD camera. The difficulty in quantifying the width of a single fibril engulfed in a dense fibrillar network led us to obtain micrographs under dilute conditions. The hydrogels were also aged overnight at room temperature to ensure well-formed fibrillar morphologies. For TEM, self-supporting, incubated hydrogels at 1 wt % were diluted 20−30 times with deionized water. A 5 μL aliquot of the diluted gel was placed on a 400 mesh carbon-coated Cu grid with the excess blotted by Whatman filter paper, and 5 μL of 1 wt % uranyl acetate solution in deionized water was then added onto the grid. Uranyl acetate is commonly used as a negative stain in TEM for contrast enhancement. Excess stain was blotted off, and the grids were dried for a minimum of 1 h prior to imaging. All fibril width measurements from TEM images were carried out using ImageJ.[75] In case of the twisted fibrils, all fibril diameters were measured from the bright areas on the fibrils in the micrograph, while the pitch was calculated as twice the distance from the center of one bright area to that of another bright area on the fibril.

Atomic Force Microscopy. Peptide solutions (1 wt %) aged overnight were diluted with deionized water to obtain a final concentration of ∼0.03 wt %, and 5 μL of the diluted fibrillar solution was applied to a freshly cleaved mica surface followed by washes with five aliquots each of 200 μL of deionized water to remove any excess salt. The samples were subsequently dried with a slow stream of N$_2$. Imaging was carried on a Digital Instruments Multi Mode Nanoscope IIIA atomic force microscope in tapping mode with a scan rate of 0.75 Hz and a resonance frequency of 300 kHz. High-frequency silicon tips (Budget Sensor BSTap300Al, force constant 40 N/m) were used for imaging. The fibril height was calculated using the section analysis feature that is a part of the Digital Instruments software. A statistical mean and standard deviation of the fibril height are reported as well. In the case of the twisted fibrils, the height measurements were carried out in the bright areas, corresponding to a slight increase in the height.

Small-Angle Neutron Scattering. SANS experiments were performed on the 30 m instrument (NG-3)[76] at the National Center for Neutron Research (NCNR), National Institute of Standards and Technology (NIST), Gaithersburg, MD. A monochromated neutron beam wavelength ($\lambda = 6$ Å) with a wavelength spread ($\Delta\lambda/\lambda$) of 0.14 was used. The scattered neutrons were captured on a 64 cm × 64 cm 2-D detector. Varying sample-to-detector distances of 1.33, 4, and 13.19 m enabled the study of the scattering wavevector q in the range $0.004 < q$ (Å^{-1}) < 0.1. The raw data were corrected for background electronic noise and radiation, detector inhomogeneity and sensitivity, and empty cell scattering. Intensities were normalized to an absolute scale relative to main beam transmission measurements through the sample and were reduced according to a published protocol.[77] The error bars of the data points for all SANS plots are within the limits of the symbols. A least-squares analysis method, used to fit the SANS data in the Guinier region, provided the reported standard deviation in the rod diameters.

Supporting Information Available: Representative analytical HPLC chromatograms, ESI-MS spectra of purified SSP1 and SSP2 as well as FTIR, WAXS, and SANS data of 1 wt % SSP1 and SSP2 hydrogels. This material is available free of charge via the Internet at http://pubs.acs.org.

JA710295T

(75) Rasband, W. S. *ImageJ*; U. S. National Institutes of Health: Bethesda, MD, 1997−2006; http://rsb.info.nih.gov/ij/.
(76) Glinka, C. J.; Barker, J. G.; Hammouda, B.; Krueger, S.; Moyer, J. J.; Orts, W. J. *J. Appl. Crystallogr.* **1998**, *31*, 430−445.
(77) Kline, S. R. *J. Appl. Crystallogr.* **2006**, *39*, 895−900.